COMMUNICATIONS IN SCIENCE AND TECHNOLOGY
Homepage: cst.kipmi.or.id

Study of green reductant effects of highly reduced graphene oxide production and their characteristics

Uswatul Chasanah[a], Wega Trisunaryanti[a,]*, Haryo Satriya Oktaviano[b], Triyono[a], Iman Santoso[c] Dyah Ayu Fatmawati[a]

[a]*Department of Chemistry, Faculty of Mathematics and Natural Sciences, Universitas Gadjah Mada, Yogyakarta, 55281, Indonesia*
[b]*Research & Technology Center, PT. Pertamina (Persero), DKI Jakarta 12950, Indonesia*
[c]*Department of Physics, Faculty of Mathematics and Natural Sciences, Universitas Gadjah Mada, Yogyakarta 55281, Indonesia*

Article history:
Received: 7 August 2022 / Received in revised form: 26 September 2022 / Accepted: 29 September 2022

Abstract

The study of the green reductant effects to produce reduced graphene oxide (rGO) has been successfully completed. The reduction of graphene oxide (GO) was carried out chemically using various reductants such as ascorbic acid (rGO-AA), gallic acid (rGO-AG), and trisodium citrate (rGO-NS). The GO was prepared using the Tour method at a temperature of 65°C for 6 hours with potassium permanganate: graphite weight ratio 1:3.5. The results showed that rGO-AA had the highest electrical conductivity value of 755.70 S/m with a number of characteristics such as a surface area of 255.93 m^2/g, total pore volume of 0.61 cm^3/g, average pore diameter of 7.10 nm, I_D/I_G ratio of 1.93, and three graphene layers in the material nanostructure stack. Therefore, it can be concluded that the reduction of GO with ascorbic acid (rGO-AA) is the most effective in producing rGO.

Keywords: Ascorbic acid; gallic acid; green reductant; reduced graphene oxide; trisodium citrate

1. Introduction

Graphene is two-dimentional (2D) carbon material that has big potential for electrodes bases on its ability to form a free-standing film without any addition of a binder agent [1,2]. Because it has unique electronic, thermal, mechanical and chemical properties, graphene has potential engineering applications in many fields, especially energy. It is widely used as a support material for electrode, especially in devices where energy is converted (fuel cells) and stored (batteries and supercapacitors) [3]. Despite the advantages explained above, graphene also has some disadvantages. These are the synthesis of large quantities of graphene and it is quite difficult to control the particle size during synthesis [4]. It is also very difficult to make composites of graphene sheets with conductive polymers or metal oxides. To overcome these difficulties, studies on malleable graphene structures have been carried out. Therefore, modified graphene, which is a derivative of graphene (graphene oxide (GO), reduced graphene oxide (rGO)), will replace pure graphene in potential applications [3].

Graphene oxide (GO) is used for graphene synthesis and has a carbon atoms monolayer with covalently connected oxygen-containing groups [5]. The synthesis of graphene can be done by biological, chemical, and physical techniques. All of them have various strategies to isolate single graphene sheets with or without changing their properties, and to synthesize a graphene oxide reduction [6–8].

Chemical exfoliation method can be used for high quality graphene synthesis from graphite [9]. The addition of potassium chlorate ($KClO_3$) and nitric acid (HNO_3) provided an increase in the weight of the sample due to the incorporation of hydrogen (H) and oxygen (O) was published by Benjamin Collins Brodie [10], the use of sulfuric acid (H_2SO_4) and a high amount of potassium chlorate ($KClO_4$) was reported by Staudenmaier [11]. Meanwhile, Hummers and Offeman [12] proposed the use of potassium permanganate ($KMnO_4$) and sulfuric acid as reagents. The H_2SO_4 acts as solvent to transport the oxidant into the graphite interlayers and an intercalation agent stabilizing the oxidant [13]. Marcano et al. [14] developed the study without $NaNO_3$ on the differences among the Hummers method, modified Hummers method, and improved Hummers method. In 2010, Tour et al. [15] reported an improvement in the Hummers method using ice instead of liquid water to prevent the high-temperature rise thus promoting better and easier control of the process, and increasing the yield and degree of oxidation, and introducing phosphoric acid (H_3PO_4) to promote the retention of carbon rings in the basal. The difference of Tour method with other methods is based on mixturing H_2SO_4 and H_3PO_4 (9:1 v/v) and further oxidation of graphite by $KMnO_4$ [16]. The advantages of Tour method are to produce a more oxidized graphite oxide with a more regular carbon framework and larger sheet size, eliminates the production of toxic gases [17] and produce more heavily oxidized hydrophilic GO [18,19].

* Corresponding author.
Email: wegats@ugm.ac.id
https://doi.org/10.21924/cst.7.2.2022.906

The hydrogen sulfide (H_2S) was first known reducing agent introduced in 1934 that has large number of reductans to reduce GO. Among these, hydrazine ($N_2H_4.H_2O$) is the best-known reductant in terms of giving rGO with improved electrical and structural properties resembling pristine graphene to a large extent. However, hydrazine is toxic reductant so many researchers have to find alternative reducing agents with qualities comparable to hydrazine. Reductant such as hydrazine, sodium borohydride, hydroquinone, and hydrohalic acid are also known as toxic reductant in rGO so they cannot be used in biochemical applications [20]. One such problem, which has led to the introduction of the "green reduction" approach in this field is the toxic nature of hydrazine to both the environment and the living organisms [21].

RGO has several properties such as good catalyst-support interaction, mesoporous structure, good electrical conductivity, large surface area, and good corrosion resistance that can be used for support materials that can strongly influence durability, electrocatalyst performance, and efficiency in polymer electrolyte membrane fuel cells [22]. The other application of rGO is the combination of metal oxide and rGO that can improve chemical functionality and compatibility as chemical sensors [23].

Materials that can also be used as reducing agents include green tea extract [24], *Chrysanthemum* [25], carrot extract [26], orange peel [27], pomegranate [28], *Lycium barbarum* [29], *Azotobacter chroococcum* [30], sodium citrate [31], caffeic acid [32], ascorbic acid [33], glycine [34], alanine [35], and bovine serum albumin [36], or gallic acid [37]. The use of ascorbic acid as a reducing agent, compared to other green reducing agents, has a conductivity value that is almost similar to that of hydrazine [38].

The above reductants that have higher conductivity than others are gallic acid, sodium citrate, and ascorbic acid. Gallic acid (3,4,5- trihydroxyl-benzoic acid) is a polyphenol naturally found in fruits (graphes, strawberries, bananas) and various plants (oak bark, tea leaves, gallnut) [39]. This molecule has been used in reducing and stabilizing agents in nanoparticle synthesis as it contains more than two hydroxyl groups that can reduce metal ions [40,41]. Ascorbic acid has been widely used as a reducing agent in the synthesis process of nanomaterials such as metal oxide and metal nanoparticles [42,43]. Sodium citrate is simultaneously used as an environmentally friendly reducing agent for the effective reduction of both GO and good size distribution [44].

Conductivity rGO with ascorbic acid that has been synthesized by Xu et al [45] is 733 S/m. The method is used with other reductant (galic acid and sodium citrate) with an expectation that it can improve their conductivy.

The first known environmentally friendly reducing agent is ascorbic acid (2010) that has been verified to be the best alternative to toxic hydrazine and is being studied currently [46]. This study is mainly focused on the chemical reduction of GO by ascorbic acid, gallic acid, and sodium citrate, which is non-toxic and affordable to produce green rGO that can be used for support material of catalyst in PEMFC.

2. Materials and Methods

2.1. Materials

Hydrochloric acid (HCl) (Merck), sulfuric acid (H_2SO_4) (Merck), graphite (Merck), phosphoric acid (H_3PO_4) (Merck), potassium permanganate ($KMnO_4$) (Merck), hydrogen peroxide (H_2O_2) (Merck), silver nitrate ($AgNO_3$) (Merck), barium chloride ($BaCl_2$) (Merck), ascorbic acid (Merck), trisodium citrate (Merck), gallic acid (Merck), ammonia solution (Merck), ethanol (Merck), deionized water (onemed) and bi-distilled water and phosphate-buffered saline (PBS) was utilized.

2.2 Instrumentations

X-ray diffraction (XRD) (Bruker D2 Phaser diffractometer) using the Cu Kα as the irradiation (k = 0.15405 nm) at a 2θ scan range of 5–90° to detect crystal size. Fourier Transform Infrared (FTIR) (Shimadzu Prestige 21) to analyze the functional group of graphene oxide with a range of 400–4000 cm^{-1} using KBr pellets. Scanning Electron Microscope-Energy Dispersive X-ray (SEM-EDX, JEOL JSM-6510) to show the surface morphology of graphene oxide and C/O ratio. Transmission electron microscopy (TEM, JEOL JEM-1400) to determine graphene nanosheet's structure. Raman Spectrometer (LabRAM HR Evolution, Horiba), Thermogravimetric Analyzer (Linseis, STA PT 1600), Surface Area Analyzer (JWGB Meso 112), the electronic transition condition of GO was measured by UV-Vis Spectrophotometer 1800 from Shimadzu Scientific and LCR meter (EUCOL U2826),

2.3 Procedure

2.3.1 Synthesis of graphene oxide

Our method was adapted from Chasanah's method [47] with certain crucial modifications. Initially, graphite flakes and $KMnO_4$ (1:3.5 w/w) were mixed in a mortar and pestle for 5 minutes and kept at a temperature below 5°C. A separate solution of H_2SO_4 and phosphoric acid H_3PO_4 (9:1 v/v) was prepared and kept at a temperature below 5°C. The acid solution was then added to the mixture of graphite flakes and $KMnO_4$ with continuous stirring (using a magnetic stirrer). Once being obtained, the solution was heated at 65°C and left for 6 h with continuous stirring. After 6 h, the solution was allowed to cool until reaching a room temperature. This was then added to a beaker containing 200 ml of deionized water ice. The mixture was added 4 ml of H_2O_2 while stirring. The mixture was washed with HCl (2x) and ethanol (2x) with intermediate centrifugation (at 5,000 rpm for 5 minutes). The precipitate was washed with PBS until pH 7. The neutral solution was checked by $AgNO_3$ and $BaCl_2$ to detect the presence of SO_4^{2-} ion and the presence of Cl^- ion, respectivelly. If it formed white precipitate in the mixture, the solution was washed again using aquabidest until it was free of impurities. After the solution was impurities free, the solution was centrifuged again at 5000 rotations per minute (rpm) for 5 minutes to split the precipitate and solution. The precipitate formed was dried at 70°C for 24 hours.

2.3.2 Synthesis reduced graphene oxide

Synthesis rGO was adapted from Xu's method [45] .GO suspension (300 mL, 0.1 $mg{\cdot}mL^{-1}$) and ascorbic acid (AA) (300 mg) were mixed, and then ammonia solution (25% w/w) was added to adjust the pH of the suspension to 9–10. After 30

min of sonicated, the GO suspension was heated to 95°C under stirring for 2 h, resulting in rGO. The produced rGO, designated as rGO-AA, was then washed process with distilled water until it became neutral. The process was repeated with a different reductant such as trisodium citrate denoted as rGO-NS and gallic acid denoted as rGO-AG.

3. Results and Discussion

XRD characterization (Figure1) was used to investigate the modification of interlayer induced in graphite-related materials. Although GO and rGO were the same material based on carbon atoms, both showed a different diffractogram pattern due to differences in arrangement and the existing additional atoms. The GO diffraction pattern exhibited an intense peak around 9.78° [48], which disappeared after GO reduction. The wider peak was observed for rGO-AA at 2θ= 24.37, rGO-AG at 2θ= 25.91, and rGO-NS at 2θ= 23.04 because of removing the oxygen-containing functional groups during the chemical reduction of GO [49]. This indicated that the π-conjugated graphene structure was significantly reestablished in the synthesized rGOs (the epoxide rings opening). Apart from this, a peak (100) was observed at regions 2θ= 42.7 for GO and 2θ=42.8 (rGO-AA), 2θ= 43.2 (rGO-AG), and 2θ= 43.1 for rGO-NS [50].

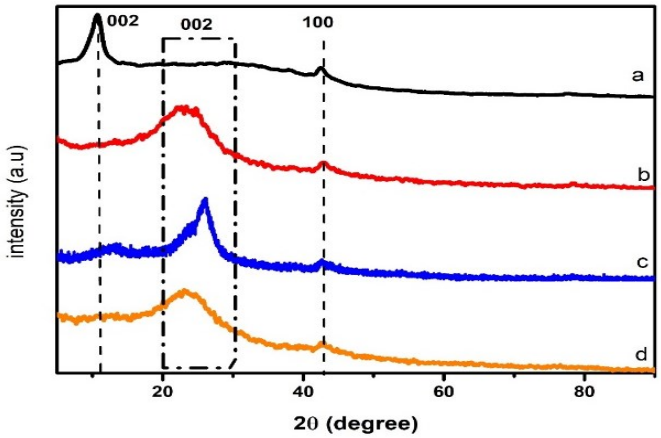

Fig. 1. Diffractogram of a) GO, b) rGO-AA, c) rGO-AG, and d) rGO-NS

Table 1. Calculation of D (average diameter), d (the average distance between graphene layers), and N (number of layers) of sample GO, rGO-AA, rGO-AG, and rGO-NS.

Material	2θ (deg)	FWHM (deg)	D (nm)	d (nm)	N
GO	9.83	1.74	4.58	0.90	5
rGO-AA	22.79	6.75	1.20	0.38	3
rGO-AG	25.87	2.67	3.05	0.34	8
rGO-NS	23.05	5.12	1.58	0.38	4

The interlayer distances (dGO > drGOs) and the number of layers (NGO < NrGOAG) (Table 1.) matched with the results in the literatur [51]; meanwhile, number of layers (NrGO-AA and NrGO-NS < NGO) matched with the literature [52]. In addition, the d-spacing of GO to all of rGO was found to decrease from 0.91 nm to 0.36 (rGO-AA), 0.34 (rGO-AG), and 0.38 (rGO-NS). This proved the efficient removal of oxygen-containing functional groups that would be matched with FTIR data. It also exposed that the thin rGO nanolayer was stacked together to form a thick bulk structure due to the presence of strong van der Waals forces between each layer [17,53–55]. After reduction, the XRD pattern of rGO was that of an amorphous material [56].

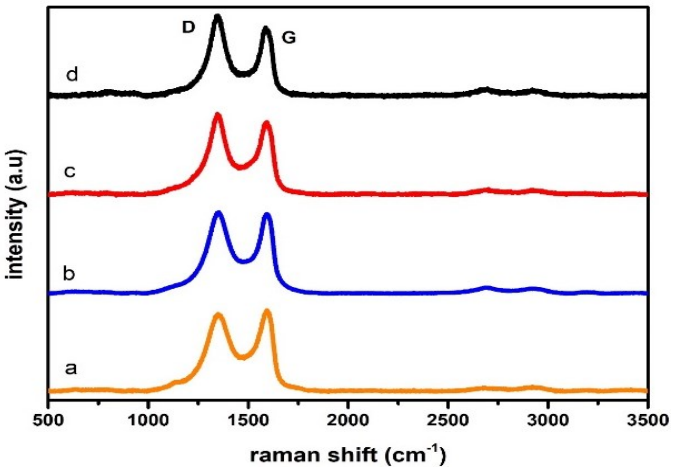

Fig. 2. Raman image of a) GO, b) rGO-AA, c) rGO-AG, and d) rGO-NS

Raman was used to determining the irregularities and defects in the crystal structure (Figure 2). The irregularity level was determined by the I_D/I_G value. The higher disorder with raising D band intensity than the G band was shown by the broadening of D and G bands [57]. The G band appeared at ~1540 cm^{-1} due to the in-plane vibrations of carbon atoms with sp^2 hybridization [58] whereas the D band appeared at ~1340 cm^{-1}, resulting from out-of-plane vibrations, which might be due to wrinkled structure and defects. Broad and short peaks ~2700 cm^{-1} attributed to the splitting of a 2D peak, which implied the increase in the number of vibrational modes due to the few-layer formation of rGO [59].

Table 2. Micro-Raman analysis of GO, rGO-AA, rGO-AG, and rGO-NS

Material	D (cm^{-1})	G (cm^{-1})	I_D/I_G
GO	1349.19	1576.96	0.78
rGO-AA	1349.19	1594.29	1.93
rGO-AG	1349.19	1590.57	1.91
rGO-NS	1347.33	1596.76	1.91

The ratio of the peak intensity of the D and G bands represented the defects in GO and rGOs (Table 2). The higher the value, the higher the defect [60]. The I_D/I_Gs of GO, rGO-AA, rGO-AG, and rGO-NS were 0.78; 1.93; 1.91; 1.91, respectively indicating that defects of rGOs were higher than GO in view of the reduction process.

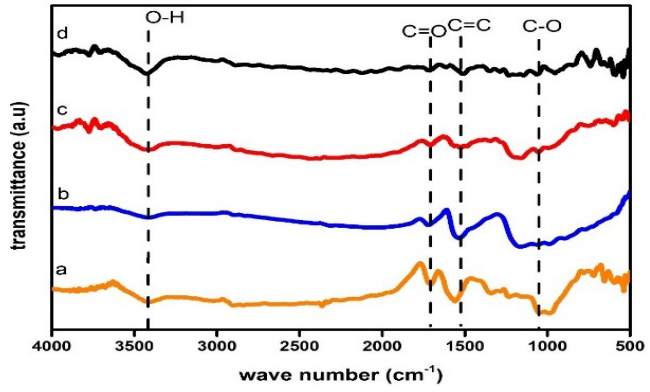

Fig. 3. FTIR spectra of a) GO, b) rGO-AA, c) rGO-AG, and d) rGO-NS

The functional group of GO and rGO and atom bonding structure based on their interaction with matter was characterized by FTIR. The vibration from the molecules were produced [61]. Figure3 presents FTIR of GO, rGO-AA, rGO-AG, and rGO-NS. The peaks at ~3400 cm^{-1} of GO, rGO-AA, rGO-AG, and rGO-NS indicated vibrations of -OH stretching. The spectrum of GO and rGOs of hydroxyl, carboxyl, and epoxy groups was present as pointed out by the characteristic peaks of the C=O stretching vibration at ~1700 cm^{-1} [51], unoxidized graphitic domain (C=C stretching) at ~1500 cm^{-1} [62]. The epoxy groups at 1140-1180 cm^{-1} (C-O stretching) [63]. After reduction (rGO-AA, rGO-AG, and rGO-NS), the peak at 1725 cm^{-1}, assigned to the C=O groups, and the peak of rGO-AA (~3391 cm^{-1}) indicated O-H vibration decreased. However, the result of FTIR data was almost same, the difference was the intensity of signal confirming to alkoxy, alcohols , and oxygen group entering this structure owing to the epoxide formation [4]. The absorption peak of GO, rGO-AA, rGO-AG, and rGO-NS can be seen in Table 3.

Table 3. The absorption peak of GO, rGO-AA, rGO-AG, and rGO-NS

Sample	Functional group (cm^{-1})			
	O-H	C=O	C=C	C-O
GO	3403.54	1703.02	1564.01	1149.32
rGO-AA	3391.97	1710.93	1517.07	1176.93
rGO-AG	3393.9	1707.03	1521.90	1158.30
rGO-NS	3424.76	1714.79	1494.89	1146.73

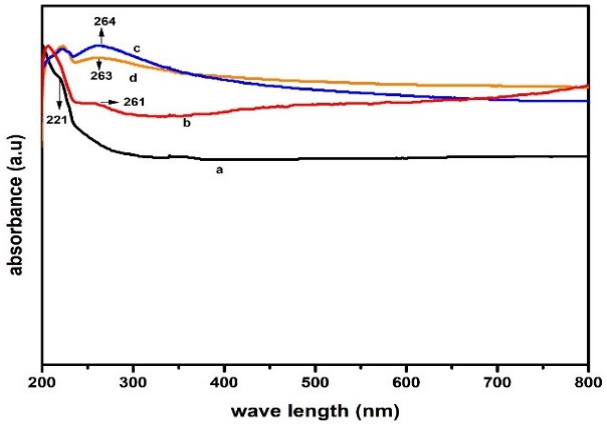

Fig. 4. UV-Vis spectra of a) GO, b) rGO-AA, c) rGO-AG, and d) rGO-NS

The transition of graphene can be measured by UV-Vis (Figure 4). The transtition of π-π* transition for C=C of graphene layers was centered at around λmax = ~220 nm [62] and the n-π* transition at around 300 nm because of the C-O > C=O groups present on the graphene sheets [15]. The UV-Vis spectrum showed a higher value of λmax for π -π* electronic transition as compared to n-π* because the π- π* transitions required less amount of energy due to the conjugation of C=C bonds of the graphene layers. After reduction (Figure 4b-c), the absorption peaks were found between ~260 nm. The UV-Vis absorption has red shift related to the increase of electron concentration and the restoration of hybridization of the sp^2 [51].

SAA was used for calculating the surface area and pore size distribution. Significant progress has been achieved lately in understanding the underlying mechanisms of adsorption in mesoporous solids, which have led to major progress in the textural characterization of porous materials by gas adsorption. The Brunauer-Emmett-Teller (BET) method is to investigate the structure, characterize the porosity of graphene, and the nitrogen adsorption-desorption isotherms [64]. Barrett-Joyner-Halenda (BJH) method is to detect the pore size distribution data are illustrated as insets in Figure 5. The GO confirms type IV isotherm according to the IUPAC classification [64], indicating that GO is a layered mesoporous structure. Also, this isotherm indicates plate-like structures with slit-shaped pores displayed by H3 hysteresis. RGO-AA, rGO-AG, and rGO-NS confirm Type II isotherm. This isotherm describes the adsorption in mesoporous materials without hysteresis [22].

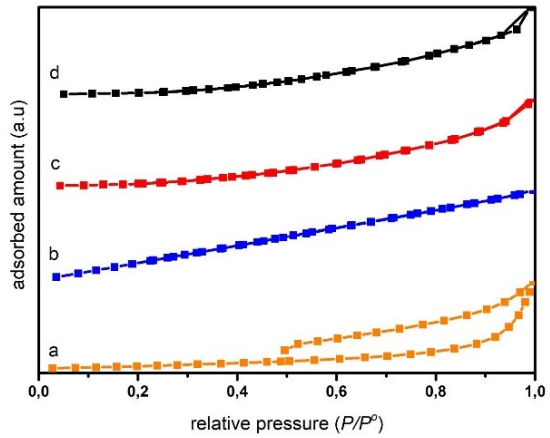

Fig. 5. Nitrogen adsorption-desorption isotherms of a) GO, b) rGO-AA, c) rGO-AG, and d) rGO-NS

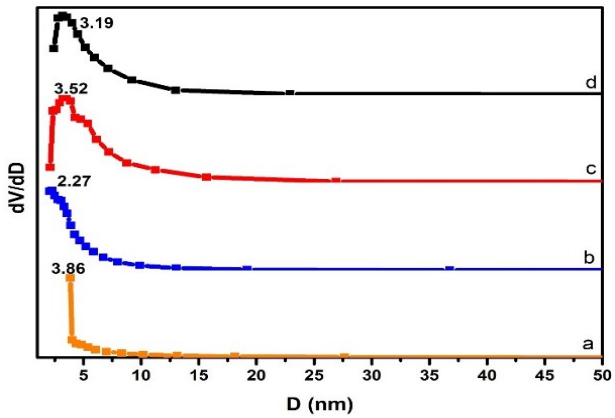

Fig. 6 Pore size distributions of a) GO, b) rGO-AA, c) rGO-AG, and d) rGO-NS

Moreover, porosity characteristics were investigated by the BJH method, and the pore size distribution curve is shown in (inset Figure 6). The pore diameter of GO, rGO-AA, rGO-AG, and rGO-NS were also found at 3.86 nm, 2.27 nm, 3.52 nm, and 3.10, respectively further confirming the microporous behavior. Moreover, rGO-AA was found to have a large BET surface area (255.93 m^2/g) with a total pore volume (0.61 cc/g) (Table 4) and a highly developed hierarchical porosity network of narrow micropores consistent with the pore size distribution mesoporous (pore size 2-50 nm) behaviors respectively. The mean pore of GO and rGOs diameter calculated by the BET method was found approximately at ~7-8 nm (Table 4). It confirmed the presence of some mesoporous characteristics formed when oxygen-containing groups are reduced with various reducing agents. During this time, irreversible agglomeration occurs due to π-π* stacking interaction and Van der Waals forces between graphene sheets. Thus, the surface area and pore volume will be reduced by the aggregation of

graphene sheets and the material obtained most probably becomes mesopores (pore size 2-50 nm) [65].

Table 4. BET analysis results of GO, rGO-AA, rGO-AG, and rGO-NS

Material	GO	rGO-AA	rGO-AG	rGO-NS
Surface area (m^2/g)	91.54	255.93	19.18	3.78
Pore diameter (nm)	7.17	7.10	7.97	8.52
Total pore volume (cc/g)	0.41	0.61	0.08	0.03

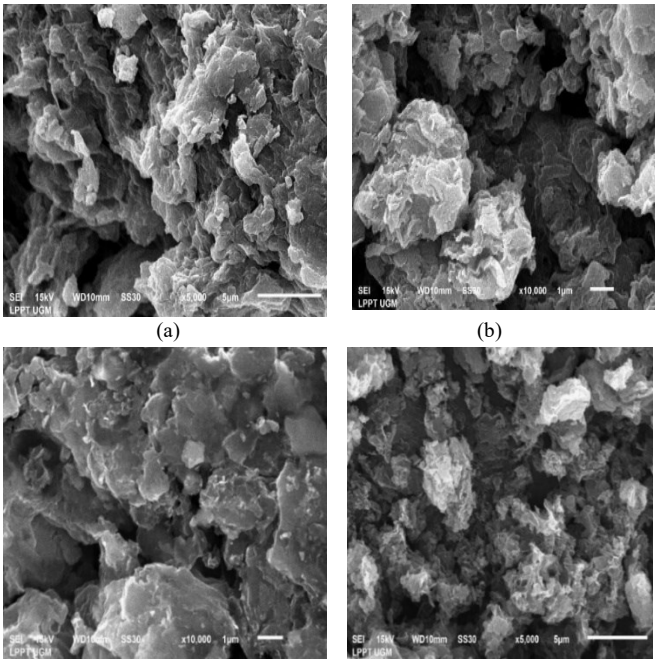

(a) (b) (c) (d)

Fig. 7. SEM images of a) GO, b) rGO-AA, c) rGO-AG, and d) rGO-NS

SEM-EDX device was used to detect the element composition and the material topography. The SEM image analyses of GO, rGO-AA, rGO-AG, and rGO-NS are given in Figure 7. All of the materials had the almost same morphology. Both GO and rGO had irregular sheet-like structures, and were randomly aggregated together, tightly connected, and overlapping [16].

Table 5. Carbon-oxygen ratio (C/O) for GO, rGO-AA, and rGO-NS

Material	%C	%O	C:O ratio
GO	55.65	45.35	1.25
rGO-AA	83,36	16.74	4.98
rGO-AG	76.40	23.60	3.23
rGO-NS	77.96	22.04	3.53

In the EDX analysis (Table 5) of the materials, the carbon-oxygen ratio (C:O) of GO which was 1.25. After reduction from GO to rGO, the C:O ratio of rGO increased to 4.98 (rGO-AA), 3.23 (rGO-AG), and 3.53 (rGO-NS). These rGOs showed that the functional groups in their structures were found less than GO. RGOs come to a structure between GO and graphene. These values was matched previous research [66] and the data were matched with FTIR data.

Table 6 presents the quantified atomic concentration of all phases and functional groups using by XPS [66] analysis. The atomic ratio of carbon to oxygen (C/O) of GO prepared by Tour method quantified by Al-Gaashani et al.'s [66] XPS was calculated to be 1.63. This ratio is in close confirming with our values calculated using EDX analysis as shown in Table 5 and Table 6. From the XPS analysis, the concentration of atomic (at %) of the oxygen-containing moieties, such as carboxyl, and carbonyl. After reducing to rGO, the C/O ratio significantly increased from 1.63 to 2.77, indicating that part of GO was successfully reduced to rGO [66]. The XPS data as confirmed by EDX data that C/O ratio from GO to rGO increased from 1.25 to 3.23- 4.98 also confirmed with XRD and FTIR data.

Table 6. Comparing XPS data by literature [66] with C/O by EDX data

Material	Peaks	Atomic conc. (%)	Phase group	C/Oby XPS	Ref.	C/O by edx
GO	(1) C1s	20.24	C-C			
	(2) C1s	35.95	C-O			
	(3) C1s	4.80	C=O			
	(4) C1s	0.97	O-C=O			
	(5) C1s	-	π-π* satellite	1.63		1.25
	(1) O1s	1.61	O-C=O			
	(2) O1s	6.06	C=O			
	(3) O1s	22.55	C-OH			
	(4) O1s	7.82	C-OC		[66]	
rGO	(1) C1s	41.76	C-C			
	(2) C1s	23.03	C-O			
	(3) C1s	5.98	C=O			
	(4) C1s	2.68	O-C=O			
	(5) C1s	-	π-π* satellite	2.77		3.23-4.98
	(1) O1s	2.13	O-C=O			
	(2) O1s	8.24	C=O			
	(3) O1s	12.53	C-OH			
	(4) O1s	3.65	C-OC			

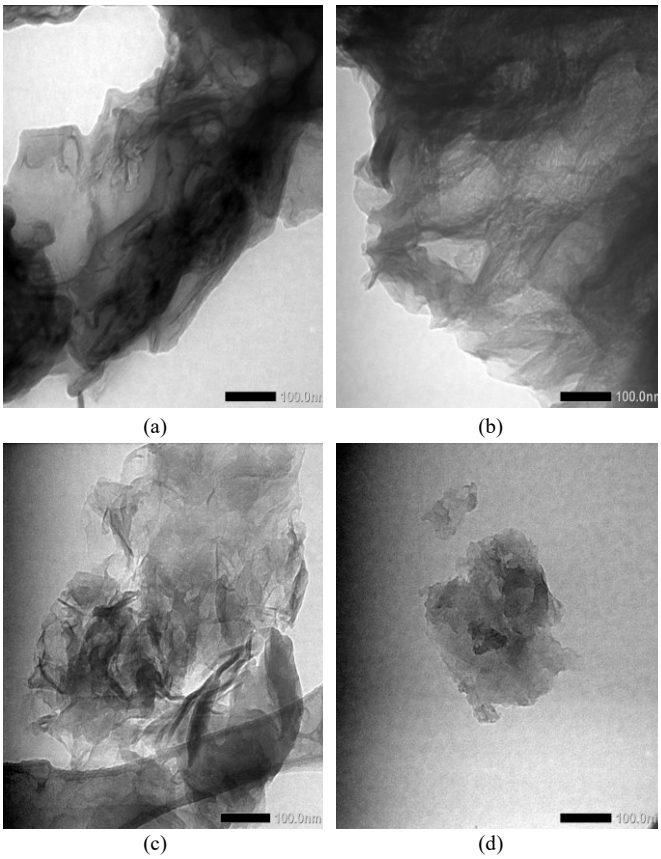

(a) (b) (c) (d)

Fig. 8. TEM images of a) GO, b) rGO-AA, c) rGO-AG, and rGO-NS

The surface studies on the morphology properties of synthesized graphene oxide and graphene were examined by TEM micrograph as shown in Figure 8. The morphology of GO and rGOs emerged as semi-transparent, which described that the material was not stable under high energy beam. Morphology GO and rGO revealed thick flat flake layers, rough surface, not crumpled, and irregular shape [67]. Moreover, unorganized particle size and irregular shape were caused by the cracking of structure that occurred during the reduction process [68].

Table 7. Conductivity calculation for GO, rGO-AA, and rGO-NS

Material	GO	rGO-AA	rGO-AG	rGO-NS
Conductivity (S/m)	$1.9x10^{-2}$	755.70	11.21	8.48

Table 7 shows the electrical properties of GO, rGO-AA, rGO-AG, and rGO-NS Good electrical conductivity is produced when only exists a small amount of oxygen functional groups [69]. As seen in Table 7 rGOs showed good electrical conductivity compared to graphene oxide (GO). RGO experienced higher conductivity than graphene oxide due to no interference in restoring the carbon sp^2 network [70]. rGO-AA was found to have the best conductivity value [21], then followed by rGO-AG and rGO-NS probably because ascorbic acid (rGO-AA), gallic acid (rGO-AG), and trisodium citrate (rGO-NS) had pKa value of 4.17; 4.50; and 6.40, respectively. The lower the pKa value, the higher the conductivity matched with the literature [71]. The factors that influence the conductivity of an acid are its strength, i.e. how much the acid dissociates in solution (how many hydrogen ions are produced) and how well the charged ions themselves conduct an electric current. Conductivity is related to ion mobility, which is higher if the ion is smaller. Furthermore, ascorbic acid has four hydroxyl groups, gallic acid has three hydroxyl groups, and trisodium citrate has only one hydroxyl group.

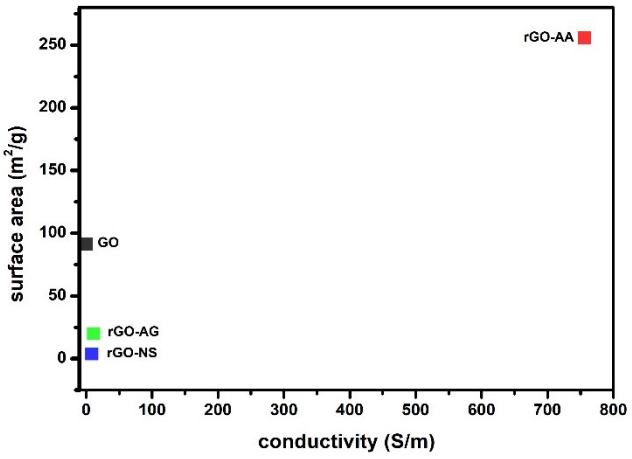

Fig. 9 Correlation between surface area and electrical conductivity

The removal of functional groups during the rapid GO reduction process increased electrical conductivity by improving orientation by repairing defects. These improved electrical conductivity values in rGOs were achieved due to the increase in surface area, as can be seen in Figure 9. [72]. The efficiency of the reduction process varies the surface area of a graphene derivative and its associated conductivity due to different populations of oxygen functional group [73–75]. Based on this fact, rGO with lower electrical conductivity has a higher proportion of oxygen-containing fractions [76]. It can be concluded that the functional groups in the rGO samples contributed to different surfaces with defect-induced carbon atoms. This would be the basis for obtaining structurally adapted properties [72]. Ascorbic acid (rGO-AA) is a stronger reducing agent than gallic acid (rGO-AG) and trisodium citrate (rGO-NS).

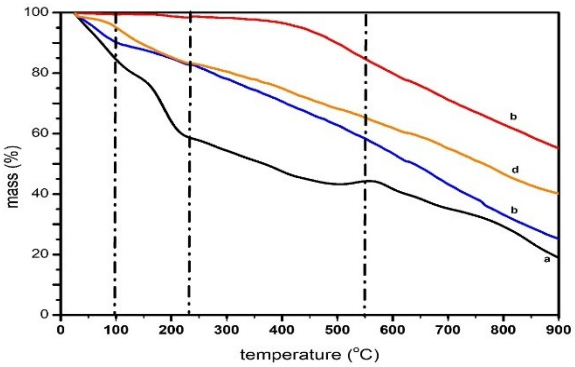

Fig. 10. TGA profile of a) GO, b) rGO-AA, c) rGO-AG, and d) rGO-NS

TGA has been used to characterize the elimination of bulk oxygen group content. Figure 10 shows the TGA curves of the GO and rGO material under a nitrogen atmosphere with a heating rate of 10°C/min. The TGA curve of the GO showed a lower apparent mass loss at 100°C, which is thought to be due to evaporation of absorbed water due to the higher hydrophobicity of the GO sample [77]. The other mass loss at 101-225°C indicated the removal of less stable oxygenated functional groups such as epoxies and carbon dioxide. In the temperature range, 226-550°C is the pyrolysis of more stable oxygenated functions, such as carbonyl and carboxyl groups. Meanwhile, above 550°C is the decomposition of the components of material carbon [26].

Table 8. Calculation of %loss mass of GO, rGO-AA, rGO-AG, and rGO-NS

Material	% loss (≤100 °C)	%loss (101-225°)	%loss (226-550°)	%loss (551-900°)	residue
GO	15.48	25.2746	14.98	25.56	18.69
rGO-AA	9.86	7.0486	24.74	33.12	25.22
rGO-AG	0.55	1.0326	13.79	29.58	55.05
rGO-NS	4.96	11.5135	18.26	25.14	40.12

The GO showed a large mass loss (~19%) in the range of 100–900°C; while rGO-AA (~25%), rGO-AG (~55%) and rGO-NS (~40%) have been attributed to the loss of oxygen functional groups [77] (see Table 8). This showed that more oxygen-containing functional groups of rGO-AG were removed by heat treatment, resulting in higher thermal stability than that followed by rGO-NS and rGO-AA. The improvement in thermal stability became more dramatic with varying reducing agent. Additionally, it can be seen that rGO-AA had a much larger mass loss than rGO-AG and rGO-NS, which were inconsistent with FTIR, conductivity, EDX and SAA results, possibly due to unstable inert gas flow in the device. Nevertheless, all rGO samples exhibited greater loss of oxygen functional groups than GO [78].

4. Conclusion

Graphene oxide was successfully prepared in our experiment by means of Tour method. The reduction of GO by various reductants such as ascorbic acid, gallic acid, and

trisodium citrate produced rGO-AA, rGO-AG, and rGO-NS, respectively. The atomic C/O ratio of GO increased from 1.25 to 4.98 (rGO-AA), 3.23 (rGO-AG), and 3.53 (rGO-NS) very close to the theoretically calculated value. Most of the hydroxyl (-OH) groups can be removed from the surface of GO using ascorbic acid (rGO-AA) and form a C=C structure, leading to the electrical conductivity of GO increasing from $1.9x10^{-2}$ to 755.70 S/m. However, the –OH groups bonded to the surface of GO could not be optimally reduced by gallic acid (rGO-AG) and trisodium citrate (rGO-NS), matching with electrical conductivity just increase 11.21 and 8.48 S/m, respectively. Additionally, some C–H still existed in RGOs. This result was also validated by SAA. The surface area of GO was 91.53 m^2/g increased by 255.93 m^2/g (rGO-AA) but the result of rGO-AG and rGO-NS were 19.18 and 3.78 m^2/g, respectively. From the XRD data, GO had five layers that could be reduced by ascorbic acid (rGO-AA) to three layers and trisodium citrate (rGO-NS) to four layers but using gallic acid (rGO-AG) it had outlier data (eight layers). The I_D/I_Gs of GO, rGO-AA, rGO-AG, and rGO-NS were 0.78; 1.93; 1.91; 1.91, respectively indicating that defects of rGOs were higher than GO because of the reduction process. The absorption peak of GO centered at around λmax = ~220 nm and shoulder was observed at around 300 nm, and the absorption peaks were found between ~260 nm after reduction (rGOs). The GO exhibited a major mass loss (~19%) in the range of 100–900°C; meanwhile, rGO-AA (~25%), rGO-AG (~55%), and rGO-NS (~40%) have been attributed to the loss of oxygen functional groups. Moreover, it can be seen that rGO-AA had much more mass loss than that of rGO-AG and rGO-NS which were contradictive with FTIR, conductivity, EDX, and SAA results. All of the materials had almost the same morphology from SEM and TEM analysis. Therefore, it can be concluded that the reduction of GO with ascorbic acid is the most effective in producing rGO. RGO-AA had the biggest surface area and the highest conductivity that can be used for catalyst support material in PEMFC.

Acknowledgments

The authors would like to thank the Ministry of Research and Technology/National Research and Innovation Agency of Republic Indonesia for financial support under the scheme of PMDSU research grant 2020 (Contract number: 3151/UN1/DITLIT/DIT-LIT/PT/2020 and 6/AMD/E1/KP.PTNBH/2020) and Hibah Penelitian Lintas Department funded by the Faculty of Mathematics and Natural Sciences, Universitas Gadjah Mada, with contract number: 187/J01.1.28/PL.06.02/2022

References

1. C. Huang, A. Hu, Y. Li, H. Zhou, Y. Xu, Y. Zhang et al. Room temperature ultrafast synthesis of N- and O-rich graphene films with an expanded interlayer distance for high volumetric capacitance supercapacitors. Nanoscale, 11 (2019), 16515-16522.
2. L. Huang, D. Santiago, P. Loyselle, L. Dai. Graphene-Based Nanomaterials for Flexible and Wearable Supercapacitors. Small, 14 (2018). 1-11.
3. M. Samancı. Chemically and thermally reduced graphene oxide supported Pt catalysts prepared by supercritical deposition. Int. J. Hydrog. Energy, 47 (2022), 19669-19689.
4. A.E.F. Oliveira, G.B. Braga, C.R.T. Tarley and A.C. Pereira. Thermally reduced graphene oxide: synthesis, studies and characterization. J. Mater. Sci., 53 (2018), 12005-12015.
5. S. Yang, Q. Chen, M. Shi, Q. Zhang, S. Lan, T. Maimaiti et al. Fast identification and quantification of graphene oxide in aqueous environment by raman spectroscopy. Nanomaterials, 10 (2020), 770-781.
6. Y.I. Zhang, L. Zhang and C. Zhou. Graphene and Related Applications. Acc. Chem. Res, 46 (2013), 2329-2339.
7. T.B. Prayitno. Tuning the magnetic states in AA-stacked bilayer zigzag graphene nanoribbons. Commun. Sci. Technol., 7 (2022), 73-79.
8. W. Yu, L. Sisi, Y. Yaiyan, and L. Jie. Progress in the functional modification of graphene/graphene oxide: A review. RSC. Adv, 10 (2020), 15328-15345.
9. M. T. Alshamkhani, L. K. Teong, L. K. Putri, A. R. Mohamed, P.Lahijani, M. Mohammadi. Effect of graphite exfoliation routes on the properties of exfoliated graphene and its photocatalytic applications. J. Environ. Chem. Eng., 9 (2021), 1-40.
10. B.C. Brodie, XIII. On the atomic weight of graphite. Philos. Trans. R. Soc, 149 (1859), 249–259.
11. L. Staudenmaier, Verfahren zur Darstellung der Graphitsäure, Berichte der Dtsch. Chem. Gesellschaft, 31 (1898), 1481–1487.
12. W.S. Hummers and R.E. Offeman, Preparation of Graphitic Oxide, J. Am. Chem. Soc. 80 (1958), 1339.
13. Y. Zhu, G. Kong, Y. Pan, L. Liu, B. Yang, S. Zhang et al. An improved Hummers method to synthesize graphene oxide using much less concentrated sulfuric acid. Chinese Chem. Lett. 33 (2022), 8–11.
14. D.C. Marcano, D. V. Kosynkin, J.M. Berlin, A. Sinitskii, Z. Sun, A. Slesarev et al. Improved synthesis of graphene oxide, ACS Nano, 4 (2010), . 4806–4814.
15. D.C. Marcano, D. V. Kosynkin, J.M. Berlin, A. Sinitskii, Z. Sun, A.S. Slesarev et al. Correction to Improved Synthesis of Graphene Oxide. ACS Nano, 12 (2018), 2078.
16. I. Bychko, A. Abakumov, O. Didenko, M. Chen, J. Tang and P. Strizhak. Differences in the structure and functionalities of graphene oxide and reduced graphene oxide obtained from graphite with various degrees of graphitization. J. Phys. Chem. Solids, 164 (2022), 110614.
17. A. Romero, M.P. Lavin-Lopez, L. Sanchez-Silva, J.L. Valverde and A. Paton-Carrero. Comparative study of different scalable routes to synthesize graphene oxide and reduced graphene oxide, Mater. Chem. Phys., 203 (2018), 284-292.
18. J. Chen, Y. Li, L. Huang, C. Li and G. Shi. High-yield preparation of graphene oxide from small graphite flakes via an improved Hummers method with a simple purification process. Carbon N. Y. 81 (2015), 826-834.
19. M.D.P. Lavin-Lopez, A. Romero, J. Garrido, L. Sanchez-Silva and J.L. Valverde. Influence of different improved hummers method modifications on the characteristics of graphite oxide in order to make a more easily scalable method. Ind. Eng. Chem. Res. 55 (2016), 12836-12847.
20. C.K. Chua, and M. Pumera. Chemical reduction of graphene oxide: A synthetic chemistry viewpoint. Chem. Soc. Rev, 1 (2014), 291-312.
21. K.K.H De Silva, H.H Huang, R.K Joshi, and M. Yoshimura. Chemical reduction of graphene oxide using green reductants. Carbon, 119 (2017), 190-199.
22. M. Samancı and A. Bayrakçeken Yurtcan. Chemically and thermally reduced graphene oxide supported Pt catalysts prepared by supercritical deposition. Int. J. Hydrogen Energy, 47 (2022). 19669–19689.
23. T.A. Saleh and G. Fadillah. Recent trends in the design of chemical sensors based on graphene–metal oxide nanocomposites for the analysis of toxic

species and biomolecules. TrAC, Trends Anal. Chem., 120 (2019), 115660.
24. Y. Wang, Z.X. Shi and J. Yin. Facile synthesis of soluble graphene via a green reduction of graphene oxide in tea solution and its biocomposites. ACS Appl. Mater. Interfaces, 3 (2011), 1127-1133.
25. D. Hou, Q. Liu, H. Cheng, K. Li, D. Wang and H. Zhang. Chrysanthemum extract assisted green reduction of graphene oxide. Mater. Chem. Phys., 183 (2016), 76-82 .
26. T. Kuila, S. Bose, P. Khanra, A.K. Mishra, N.H. Kim and J.H. Lee. A green approach for the reduction of graphene oxide by wild carrot root. Carbon N. Y., 50 (2012), 94-921.
27. S. Thakur and N. Karak. Green reduction of graphene oxide by aqueous phytoextracts. Carbon N. Y, 50 (2012), 5331-5339.
28. F. Tavakoli, M. Salavati-Niasari, A. Badiei and F. Mohandes. Green synthesis and characterization of graphene nanosheets. Mater. Res. Bull., 63 (2015), 51-57.
29. D. Hou, Q. Liu, H. Cheng, H. Zhang and S. Wang. Green reduction of graphene oxide via Lycium barbarum extract. J. Solid State Chem., 246 (2017), 351-356.
30. Y. Gao, J. Wu, X. Ren, X. Tan, T. Hayat, A. Alsaedi et al. Impact of graphene oxide on the antibacterial activity of antibiotics against bacteria. Environ. Sci. Nano, 4 (2017), 1016–1024.
31. W. Wan, Z. Zhao, H. Hu, Y. Gogotsi and J. Qiu. Highly controllable and green reduction of graphene oxide to flexible graphene film with high strength. Mater. Res. Bull., 48 (2013), 4797-4803.
32. Z. Bo, X. Shuai, S. Mao, H. Yang, J. Qian, J. Chen et al. Green preparation of reduced graphene oxide for sensing and energy storage applications. Sci. Rep., 4 (2014), 1-8.
33. T.F. Emiru and D.W. Ayele. Controlled synthesis, characterization and reduction of graphene oxide: A convenient method for large scale production. Egypt. J. Basic Appl., Sci. 4 (2017), 74-79.
34. S. Bose, T. Kuila, A.K. Mishra, N.H. Kim and J.H. Lee. Dual role of glycine as a chemical functionalizer and a reducing agent in the preparation of graphene: An environmentally friendly method. J. Mater. Chem., 22 (2012), 9696-9703.
35. J. Wang, E.C. Salihi and L. Šiller. Green reduction of graphene oxide using alanine. Mater. Sci. Eng. C, 72 (2017), 1-6.
36. J. Liu, S. Fu, B. Yuan, Y. Li and Z. Deng. Toward a universal “adhesive nanosheet” for the assembly of multiple nanoparticles based on a protein-induced reduction/decoration of graphene oxide. J. Am. Chem. Soc., 132 (2010), .
37. J. Li, G. Xiao, C. Chen, R. Li and D. Yan, Superior dispersions of reduced graphene oxide synthesized by using gallic acid as a reductant and stabilizer, J. Mater. Chem. A 1 (2013), 7279-7281.
38. M.J. Fernández-Merino, L. Guardia, J.I. Paredes, S. Villar-Rodil, P. Solís-Fernández, A. Martínez-Alonso et al. Vitamin C is an ideal substitute for hydrazine in the reduction of graphene oxide suspensions. J. Phys. Chem. C, 114 (2010), 6426-6432 .
39. D.Y. Kim, J. Suk Sung, M. Kim and G. Ghodake. Rapid production of silver nanoparticles at large-scale using gallic acid and their antibacterial assessment. Mater. Lett., 155 (2015), 62-64.
40. J. Lee, S. Oh, M. Jang, J. Kim, J. Lee and H. Zhou. Synthesis of silver nanoparticles using analogous reducibility of phytochemicals. Curr. Appl. Phys., 16 (2016), 738-747.
41. Y. Zhou, M. Xu, Y. Liu, Y. Bai, Y. Deng, J. Liu et al. Green synthesis of Se/Ru alloy nanoparticles using gallic acid and evaluation of theiranti-invasive effects in HeLa cells. Colloids Surfaces B Biointerfaces, 144 (2016), 118-124.
42. A. Sood, V. Arora, J. Shah, R.K. Kotnala and T.K. Jain. Ascorbic acid-mediated synthesis and characterisation of iron oxide/gold core–shell nanoparticles. J. Exp. Nanosci., 11 (2016), 370-382.
43. S. Yokoyama, K. Sato, M. Muramatsu, T. Yamasuge, T. Itoh, K. Motomiya et al. Green synthesis and formation mechanism of nanostructured Bi2Te3 using ascorbic acid in aqueous solution. Adv. Powder Technol., 26 (2015), 789-796.
44. Z. Zhang, H. Chen, C. Xing, M. Guo, F. Xu, X. Wang et al. Sodium citrate: A universal reducing agent for reduction / decoration of graphene oxide with au nanoparticles. Nano Res., 4 (2011), 599-611.
45. C. Xu, X. Shi, A. Ji, L. Shi, C. Zhou and Y. Cui. Fabrication and characteristics of reduced graphene oxide produced with different green reductants. PLoS One, 10 (2015), 1-15.
46. J. Zhang, H. Yang, G. Shen, P. Cheng, J. Zhang and S. Guo. Reduction of graphene oxide via L-ascorbic acid._Supporting Information. Chem. Commun. (Camb). 2 (2010), 112-114.
47. U. Chasanah, W. Trisunaryanti, H.S. Oktaviano And D.A. Fatmawati, The Performance Of Green Synthesis Of Graphene Oxide Prepared By Modified Hummers Method With Oxidation Time Variation, Rasayan J. Chem. 14 (2021), 2017–2023.
48. G. Fadillah, T.A. Saleh, S. Wahyuningsih, E. Ninda Karlina Putri and S. Febrianastuti. Electrochemical removal of methylene blue using alginate-modified graphene adsorbents. Chem. Eng. J., 378 (2019), 122140.
49. G. Fadillah, R. Hidayat and T.A. Saleh. Hydrothermal assisted synthesis of titanium dioxide nanoparticles modified graphene with enhanced photocatalytic performance. J. Ind. Eng. Chem., 113 (2022), 411–418.
50. M.P. Lavin-Lopez, A. Paton-Carrero, L. Sanchez-Silva, J.L. Valverde and A. Romero. Influence of the reduction strategy in the synthesis of reduced graphene oxide. Adv. Powder Technol., 28 (2017), 3195-3203.
51. M. Coros, F. Pogacean, A. Turza, M. Dan, C. Berghian-Grosan, I.O. Pana et al. Green synthesis, characterization and potential application of reduced graphene oxide. Phys. E Low-Dimensional Syst. Nanostructures, 119 (2020), .
52. J.C. Silva Filho, E.C. Venancio, S.C. Silva, H. Takiishi, L.G. Martinez and R.A. Antunes, A thermal method for obtention of 2 to 3 reduced graphene oxide layers from graphene oxide, SN Appl. Sci. 2 (2020), 113971.
53. N.M.S. Hidayah, W.W. Liu, C.W. Lai, N.Z. Noriman, C.S. Khe, U. Hashim et al. Comparison on graphite, graphene oxide and reduced graphene oxide: Synthesis and characterization. in AIP Conference Proceedings, 1892 (2017), 150092.
54. R. Siburian, H. Sihotang, S. Lumban Raja, M. Supeno and C. Simanjuntak. New route to synthesize of graphene nano sheets. Orient. J. Chem., 34 (2018), 182-187.
55. S. Sadhukhan, T.K. Ghosh, D. Rana, I. Roy, A. Bhattacharyya, G. Sarkar et al. Studies on synthesis of reduced graphene oxide (RGO) via green route and its electrical property. Mater. Res. Bull., 79 (2016), 41-51.
56. L. long Dong, W. ge Chen, N. Deng and C. hao Zheng. A novel fabrication of graphene by chemical reaction with a green reductant. Chem. Eng. J. 306 (2016), 754-762.
57. I. Srivastava, R.J. Mehta, Z.Z. Yu, L. Schadler and N. Koratkar. Raman study of interfacial load transfer in graphene nanocomposites. Appl. Phys. Lett. 98 (2011), 1-3.
58. L.M. Malard, M.A. Pimenta, G. Dresselhaus, and M.S. Dresselhaus. Raman spectroscopy in graphene. Phys. Rep., 473 (2009), 51-87.
59. I. Childres, L.A. Jauregui, W. Park, H. Caoa and Y.P. Chena. Raman spectroscopy of graphene and related materials. in New Developments in Photon and Materials Research, 19 (2013), 1-20.
60. A.C. Ferrari, J.C. Meyer, V. Scardaci, C. Casiraghi, M. Lazzeri, F. Mauri et al. Raman spectrum of graphene and graphene layers. Phys. Rev. Lett. 97 (2006), 187401.
61. V. Ţucureanu, A. Matei, and M. Avram. FTIR Spectroscopy for Carbon Family Study. Crit. Rev. Anal. Chem., 46 (2016), 502-520.

62. B.D. Ossonon and D. Bélanger. Synthesis and characterization of sulfophenyl-functionalized reduced graphene oxide sheets. RSC Adv., 7 (2017), 27224-27234.
63. G. Surekha, K.V. Krishnaiah, N. Ravi and R. Padma Suvarna. FTIR, Raman and XRD analysis of graphene oxide films prepared by modified Hummers method. in Journal of Physics: Conference Series, 1495 (2020), 1-7.
64. A. Marinoiu, M. Andrulevicius, A. Tamuleviciene, T. Tamulevicius, M. Raceanu and M. Varlam. Synthesis of well dispersed gold nanoparticles on reduced graphene oxide and application in PEM fuel cells. Appl. Surf. Sci. 504 (2020), 144511.
65. T.A. Zegeye, M.C. Tsai, J.H. Cheng, M.H. Lin, H.M. Chen, J. Rick et al. Controllable embedding of sulfur in high surface area nitrogen doped three dimensional reduced graphene oxide by solution drop impregnation method for high performance lithium-sulfur batteries. J. Power Sources, 353 (2017), 298-311.
66. R. Al-Gaashani, A. Najjar, Y. Zakaria, S. Mansour and M.A. Atieh. XPS and structural studies of high quality graphene oxide and reduced graphene oxide prepared by different chemical oxidation methods. Ceram. Int. 45 (2019), 14439-14448.
67. A.K. Mishra and S. Ramaprabhu. Functionalized graphene-based nanocomposites for supercapacitor application. J. Phys. Chem. C 115 (2011), 14006-14013.
68. X.M. Wang, M.E. Wang, D.D. Zhou and Y.Y. Xia. Structural design and facile synthesis of a highly efficient catalyst for formic acid electrooxidation. Phys. Chem. Chem. Phys., 13 (2011), 13594-13597.
69. A. Shalaby, D. Nihtianova, P. Markov, A.D. Staneva, R.S. Iordanova and Y.B. Dimitriev. Structural analysis of reduced graphene oxide by transmission electron microscopy. Bulg. Chem. Commun., 47 (2015), 291-295.
70. Y. Geng, S.J. Wang and J.K. Kim. Preparation of graphite nanoplatelets and graphene sheets. J. Colloid Interface Sci., 336 (2009), 592-598.
71. Y. Zhang, Z. Chu, C.A. Dreiss, Y. Wang, C. Fei and Y. Feng. Smart wormlike micelles switched by CO2 and air. Soft Matter, 9 (2013), 6217-6222.
72. V.B. Mohan, K. Jayaraman and D. Bhattacharyya. Brunauer–Emmett–Teller (BET) specific surface area analysis of different graphene materials: A comparison to their structural regularity and electrical properties. Solid State Commun., 320 (2020), 114004.
73. V.B. Mohan, L. Jakisch, K. Jayaraman and D. Bhattacharyya. Role of chemical functional groups on thermal and electrical properties of various graphene oxide derivatives: A comparative x-ray photoelectron spectroscopy analysis. Mater. Res. Express, 5 (2018), 1-8.
74. J. Światowska, V. Lair, C. Pereira-Nabais, G. Cote, P. Marcus and A. Chagnes. XPS, XRD and SEM characterization of a thin ceria layer deposited onto graphite electrode for application in lithium-ion batteries. Appl. Surf. Sci., 257 (2011), 9110-9119.
75. S. Park, J. An, J.R. Potts, A. Velamakanni, S. Murali and R.S. Ruoff. Hydrazine-reduction of graphite- and graphene oxide. Carbon N. Y., 49 (2011), 3019-3023.
76. S. Eigler, M. Enzelberger-Heim, S. Grimm, P. Hofmann, W. Kroener, A. Geworski et al. Wet chemical synthesis of graphene. Adv. Mater., 25 (2013), 3583-3587.
77. S. Jin, Q. Gao, X. Zeng, R. Zhang, K. Liu, X. Shao et al. Effects of reduction methods on the structure and thermal conductivity of free-standing reduced graphene oxide films. Diam. Relat. Mater., 58 (2015), 54-61.
78. T.H.T. Vu, T.T.T. Tran, H.N.T. Le, P.H.T. Nguyen, N.Q. Bui and N. Essayem. A new green approach for the reduction of graphene oxide nanosheets using caffeine. Bull. Mater., Sci. 38 (2015), 667-671.